

Low-Frequency Measurements of Seismic Velocity and Attenuation in Antigorite Serpentine

Emmanuel C. David¹, Nicolas Brantut¹, Lars N. Hansen², and Ian Jackson³

Laboratory measurements of seismic velocity and attenuation in antigorite serpentinite at a confining pressure of 2 kbar and temperatures up to 550 °C (*i.e.*, in the antigorite stability field) provide new results relevant to the interpretation of geophysical data in subduction zones. A polycrystalline antigorite specimen was tested via forced-oscillations at small strain amplitudes and seismic frequencies (mHz–Hz). The shear modulus has a temperature sensitivity, $\partial G/\partial T$, averaging $-0.017 \text{ GPa K}^{-1}$. Increasing temperature above 500 °C results in more intensive shear attenuation (Q_G^{-1}) and associated modulus dispersion, with Q_G^{-1} increasing monotonically with increasing oscillation period and temperature. This “background” relaxation is adequately captured by a Burgers model for viscoelasticity and possibly results from intergranular mechanisms. Attenuation is higher in antigorite ($\log_{10} Q_G^{-1} \approx -1.5$ at 550 °C and 0.01 Hz) than in olivine ($\log_{10} Q_G^{-1} \ll -2.0$ below 800 °C), but such contrast does not appear to be strong enough to allow robust identification of antigorite from seismic models of attenuation only.

1. Introduction

The interpretation of geophysical data and the associated need to provide constraints on the presence of serpentinites, notably in subduction zones, has motivated a number of laboratory studies reporting measurements of P- and S-wave velocities under controlled conditions of pressure and temperature, on both single-crystal [Bezacier *et al.*, 2010, 2013] and polycrystalline serpentinites [see *e.g.* Birch, 1960; Christensen, 1978; Kern *et al.*, 1997; Watanabe *et al.*, 2007; Ji *et al.*, 2013; David *et al.*, 2018]. However, geophysical observations of *seismic attenuation* (or its inverse, the quality factor Q) in subduction zones [see *e.g.* Eberhard-Phillips *et al.*, 2008; Pozgay *et al.*, 2009; Wang *et al.*, 2017] have generally defied conclusive interpretation because of the crucial lack of directly relevant laboratory data for serpentinites. Correlations between low- Q anomalies and serpentinitization are usually based on joint information from velocity tomography and the commonly held view that the presence of serpentinites is associated with low velocities and high Poisson’s ratio [Hyndman and Peacock, 2003]. Ultrasonic velocity measurements demonstrate that while this correlation might be appropriate for lizardite or chrysotile serpentinites, it is not valid for antigorite serpentinites [Christensen, 2004;

Reynard, 2013; David *et al.*, 2018]. In addition, seismic attenuation (particularly shear attenuation) is very sensitive to many factors, including temperature, grain size, dislocation density, melt fraction and redox conditions [see *e.g.* Jackson, 2015; Cline *et al.*, 2018].

Among the serpentine group, antigorite is the mineral stable over the widest depth range [Ulmer and Trommsdorff, 1995]. The only existing, published attenuation data in serpentinites were reported on an anisotropic antigorite serpentinite by Kern *et al.* [1997], who measured the directional dependence of ultrasonic P- and S-wave velocities and their associated attenuations up to 6 kbar confining pressure and 700 °C. More recently, Svitek *et al.* [2017] performed similar measurements for P-waves up to 4 kbar confining pressure. However, such attenuation (and velocity) data were only obtained at the single MHz frequency of the ultrasonic pulse transmission method, which limits seismological application of the results as most rocks exhibit solid-state viscoelastic relaxation at lower frequencies, notably when temperature is increased [Jackson, 2015].

This lack of data motivated the present laboratory study for measuring shear modulus and attenuation on an isotropic antigorite specimen. The use of forced-oscillation techniques allows for mechanical spectroscopy in the mHz–Hz frequency range and under low strain amplitudes ($< 10^{-5}$) analogous to those of seismic wave propagation. Measurements were carried out in the “Jackson-Paterson” gas medium apparatus [Jackson and Paterson, 1993], from room temperature to 550 °C, in the antigorite stability field. The applied confining pressure of 2 kbar is expected to be sufficient to suppress most of the contribution from open microcracks (as demonstrated by a recent study on the same material by David *et al.* [2018]) or from other effects arising from frictional sliding on crack surfaces and grain boundaries [Mavko, 1979; Jackson *et al.*, 1992]. Additional measurements under flexural forced oscillation, providing access to Young’s modulus and associated attenuation, are also reported at selected temperatures. Discussion of the results focuses on the temperature-dependence of shear modulus, on the possible mechanisms responsible for the observed viscoelastic relaxation, and on a comparison with existing data on olivine followed by concluding remarks on the geophysical significance of the new laboratory data.

2. Experimental Materials and Methods

A specimen was cored from a block of “Vermont antigorite serpentinite” acquired from Vermont Verde Antique’s Rochester quarry (Vermont, USA). This block is the same material as the “isotropic” block described in detail in David *et al.* [2018]. The rock is nearly pure antigorite ($> 95\%$), with minor amounts of magnetite and magnesite (both at about 2% level). The antigorite grains are extremely heterogeneous in both size and shape (Figure 1a). The material is mainly fine-grained, but grain size ranges from sub-micron to a few hundreds of microns. The antigorite grains are generally elongated with random orientations of their long axes. The rock is elastically isotropic, with P- and S-wave velocities averaging 6.5 and 3.7 km s^{-1} , respectively, at room pressure and temperature. Rock density is $2.65 \times 10^3 \text{ kg m}^{-3}$.

¹Department of Earth Sciences, University College London, London, United Kingdom.

²Department of Earth Sciences, University of Oxford, Oxford, United Kingdom.

³Research School of Earth Sciences, Australian National University, Canberra, Australia.

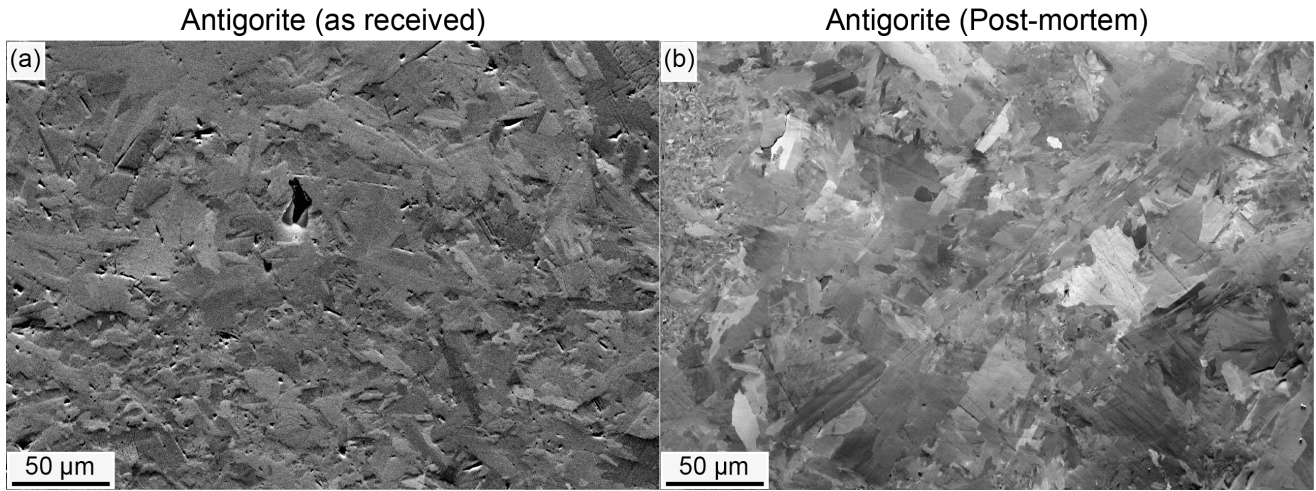


Figure 1. Forescatter electron images of antigorite. a) Specimen as received (after *David et al.* [2018]); b) Transverse section of specimen recovered post-mortem after exposure to a maximum temperature of 550 °C. The forescatter electron images were acquired using the Oxford Instruments AZtec software on an FEI Quanta 650 field-emission gun scanning-electron microscope in the Department of Earth Sciences at the University of Oxford.

The cylindrical core specimen was then precision ground to 11.50 mm in diameter and 31.14 mm in length and clamped between a series of optically flat LucaloxTM alumina pistons (see Figure 1 of *Jackson et al.* [2009]). This assembly was enclosed within a thin-walled (0.35 mm) copper jacket and loaded into the “Jackson-Paterson” gas apparatus at the Australian National University (Canberra, Australia) for high-temperature mechanical testing using low-frequency forced oscillations [*Jackson and Paterson*, 1993]. The specimen was pressurised to a confining pressure of 2 kbar for the entire experiment. Temperature was then raised in 50 °C intervals to the maximum targeted temperature of 550 °C. This maximum temperature was chosen to conservatively cover most of the antigorite stability field while avoiding dehydration [*Ulmer and Trommsdorff*, 1995]. The specimen was annealed for 2 h at 550 °C and then staged-cooled in 50 °C intervals down to room temperature using the same ramp as for staged-heating (450 °C h⁻¹). After completion of the experiment, examination of microstructures in the sectioned antigorite specimen (Figure 1b) indicates that the staged heating, exposure to annealing at 550 °C and subsequent staged cooling have resulted in no measurable microstructural evolution relative to the starting material (Figure 1a), with no evidence of dehydration.

Torsional forced-oscillation tests were conducted at a series of ten logarithmically equispaced periods between 1 and 1000 s, at selected temperatures, during *both* staged heating and staged cooling. It was observed that the mechanical behaviour during staged heating and cooling was reproducible, which is consistent with the absence of microstructural evolution during the entire experiment. Here we only report data obtained during *staged cooling*, as we consider those to be the most representative of the stable microstructure. Several forced-oscillation tests were performed at 500 °C to check for both temporal evolution and amplitude dependence of the mechanical behaviour (Figures A.1a and A.1b). The reason for conducting such tests at 500 °C, rather than at the maximum temperature of 550 °C, was again to avoid any dehydration in the antigorite specimen. The mechanical behaviour was unaffected by increasing exposure time (Figures A.1a and A.1b), a result that is again consistent with the absence of microstructural evolution in the antigorite specimen. However, the mechanical response (particularly the shear modulus) was amplitude-dependent for applied shear stresses above 1200 kPa (Figures A.1a and A.1b), corresponding to maximum shear strains $\gtrsim 1.5 \times 10^{-5}$ in the

antigorite specimen. Accordingly, in order to maximise the signal to noise ratio whilst satisfying the condition of linear viscoelastic behaviour, a shear stress amplitude of 1200 kPa was used during staged cooling to room temperature.

At a given temperature and oscillation period, a sinusoidally time-varying torque was applied by a pair of electromagnetic drivers located at the lower end of the assembly (see *e.g.* Figure 1a of *Cline and Jackson* [2016]). Time-varying displacements were measured by pairs of parallel-plate capacitance transducers mounted off-axis for mechanical advantage. Examples of raw data are given in *Jackson and Paterson* [1993]. The procedure for estimation of shear modulus (G) and attenuation (Q_G^{-1}) from torsional forced oscillation data required a parallel series of experiments to be conducted on a “reference assembly” in which the antigorite specimen is replaced by a single-crystal sapphire specimen, as described in *Jackson and Paterson* [1993]. Importantly, such procedure also involved a correction for the viscoelasticity of the copper jacket. Extensive data on small-strain viscoelasticity of copper were recently reported by *David and Jackson* [2018] for copper annealed at 1050 °C and 900 °C. It was observed that although the different annealing conditions result in substantially different grain growth in copper, there is only a modest difference in the viscoelastic behaviour. Unfortunately, no equivalent data are available for copper annealed at 550 °C. Hence, the sensitivity of the mechanical behaviour to the jacket correction was tested by comparing results obtained using the viscoelastic properties of copper annealed at 1050 and 900 °C, at selected temperatures (Figures A.1c and A.1d). The two distinct jacket corrections did not noticeably affect the period-dependence of shear modulus and attenuation (for $\log_{10}(Q_G^{-1}) \gtrsim 2.2$), and only resulted in a small offset of about 1–2 GPa for the shear modulus, which is a direct estimate of the accuracy of measurements. Accordingly, because of a denser sampling in the temperature interval ≤ 550 °C, the data of *David and Jackson* [2018] on the viscoelasticity of copper annealed to 1050 °C were used for the jacket correction in this study.

In addition to torsional oscillations, *flexural* forced-oscillation tests were conducted in the same frequency range as for torsional oscillations at selected temperatures during staged heating (20, 300 and 500 °C) by using a sinusoidally

time-varying bending force and an appropriate arrangement of the capacitance transducers for measuring bending displacements (see, *e.g.*, Figure 1c of *Cline and Jackson* [2016]). The procedure for extraction of Young's modulus (E) and its associated attenuation (Q_E^{-1}) from flexural forced-oscillation data involved forward modelling with a finite-difference filament elongation model for flexure of the long thin experimental assembly. This procedure is described in *Jackson et al.* [2011] and *Cline and Jackson* [2016].

The variation of both shear modulus and attenuation as functions of oscillation period and temperature can be fitted by a model for linear viscoelasticity based on a Burgers-type creep function [*Jackson and Faul*, 2010]. The specific features of the Burgers model used in this study are recalled here. The model incorporates a broad distribution $D_B(\tau)$ of anelastic relaxation times, τ , to account for the monotonic “background” dissipation and associated modulus dispersion as:

$$D_B(\tau) = \frac{\alpha \tau^{\alpha-1}}{\tau_M^\alpha - \tau_L^\alpha} \quad (1)$$

with $0 < \alpha < 1$ for $\tau_L < \alpha < \tau_M$ and zero elsewhere [*Minster and Anderson*, 1981]. In equation (1), the upper limit τ_M is identified with the characteristic time for Maxwell relaxation, giving way to *viscous relaxation* at sufficiently long timescales ($\gg \tau_M$). The variation of G and Q_G^{-1} with angular frequency $\omega = 2\pi/T_0$ is prescribed by

$$G(\omega) = [J_1^2(\omega) + J_2^2(\omega)]^{-1/2} \quad \text{and} \quad Q_G^{-1} = J_2(\omega)/J_1(\omega), \quad (2)$$

where $(J_1(\omega), J_2(\omega))$ are, respectively, the real and negative imaginary parts of the complex compliance $J^*(\omega)$, which are explicitly related to the distribution of relaxation times as follows [*Jackson and Faul*, 2010]

$$J_1(\omega) = \frac{1}{G_U} \left[1 + \Delta_B \int_{\tau_L}^{\tau_M} \frac{D_B(\tau)}{1 + \omega^2 \tau^2} d\tau \right], \quad (3)$$

$$J_2(\omega) = \frac{1}{G_U} \left[\omega \Delta_B \int_{\tau_L}^{\tau_M} \frac{\tau D_B(\tau)}{1 + \omega^2 \tau^2} d\tau + \frac{1}{\omega \tau_M} \right], \quad (4)$$

where G_U is the unrelaxed shear modulus and Δ_B is the relaxation strength.

The *temperature dependence* of each of the two characteristic relaxation times (τ_L, τ_M) relative to their respective values (τ_{LR}, τ_{MR}) at reference temperature T_R follows the Arrhenian expression

$$\tau_i(T) = \tau_{iR} \left[e^{(E_B/R)(1/T - 1/T_R)} \right], \quad (5)$$

where $i = L$ or $i = M$ for the broad anelastic relaxation background, associated with an activation energy E_B ; R is the gas constant. Finally, the temperature dependence of the unrelaxed shear modulus, G_U , relative to its value at the reference temperature, $G_U(T_R)$, is simply specified as

$$G_U(T) = G_U(T_R) + (T - T_R)(dG_U/dT_R). \quad (6)$$

3. Results

Experimental results for the variation of shear modulus and attenuation with oscillation period and temperature in the antigorite specimen are presented in Figure 2. Note that the reason for not conducting forced-oscillation tests at longer oscillation periods (> 101 s) at all temperatures was that shear modulus and dissipation were not found to be strongly frequency-dependent below 450 °C.

Table 1. Values for the 7 parameters of the optimal Burgers model for antigorite (see Figure 2), fitted to $N = 14$ (G, Q_G^{-1}) data pairs using a reference temperature $T_R = 500$ °C. Model misfit is $\sqrt{(\chi_G^2 + \chi_{Q_G^{-1}}^2)/(2N)} = 0.55$ with *a priori* errors of

$\sigma(G)/G = 0.03$ and $\sigma[\log_{10}(Q_G^{-1})] = 0.05$. Parameter uncertainties are parenthesised after parameter value, and parameters that are bracketed indicate that value was kept fixed for purposes of convergence in the fitting strategy.

G_U , GPa	36.6(0.5)
dG_U/dT , GPa K ⁻¹	-0.026(0.012)
Δ_B	0.13(0.01)
α	0.10(0.03)
$\log_{10}(\tau_{LR})$, s	[-1.7]
$\log_{10}(\tau_{MR})$, s	1.7(0.05)
E_B , kJ mol ⁻¹	268(21)

The shear modulus decreases systematically with increasing temperature and, at all temperatures above 300 °C, with increasing oscillation period (Figure 2a). The strength in dispersion of the shear modulus increases slightly with temperature to reach about 4% at 550 °C across the 1–100 s oscillation period interval. Below 450 °C, $\log_{10} Q_G^{-1} < -2$ and is essentially period-independent, with a tendency to increase slightly with temperature (Figure 2b); the scatter in the data provides an indication of experimental uncertainties. Increasing temperature above 500 °C results in more intensive shear attenuation, with Q_G^{-1} increasing noticeably with temperature and oscillation period. Over the observational oscillation period window, the monotonic increase of Q_G^{-1} with oscillation period T_0 above 500 °C is typical of the “absorption band” commonly observed in many rocks at elevated temperatures [*Cooper*, 2002; *Minster and Anderson*, 1981; *Jackson et al.*, 1992] and adequately approximated by a power law of the form $Q_G^{-1} \sim T_0^\alpha$ with $\alpha = 0.20$ and $\alpha = 0.26$ at 500 °C and 550 °C, respectively.

The variation of both shear modulus and attenuation with oscillation period and temperature in the 400–550 °C range is reasonably well described by a “background relaxation only” Burgers-type model for linear viscoelasticity (Figure 2; fitting parameters in Table 1). The model was fitted to the (G, Q_G^{-1}) data pairs for which Q_G^{-1} is systematically period-dependent (*i.e.*, at 500–550 °C) and extrapolated to lower temperatures. That shear modulus and dissipation data are jointly fitted by the Burgers model, based on a creep function and ensuring compliance with the linear Kramers-Kronig relations, is confirmation that the measurements were taken in the regime of linear viscoelasticity. The trends in variation of both shear modulus and dissipation with oscillation period are well captured by the model in the 400–550 °C range, but the temperature-dependence of the shear modulus becomes increasingly offset at 400 °C. Part of the misfit is attributed to the relatively sharp increase in the dissipation and associated modulus dispersion data which occurs between 450 and 500 °C. The characteristic time for Maxwell relaxation is $\log_{10}(\tau_M) = -1.7$ at 500 °C (Table 1) and $\log_{10}(\tau_M) = -0.6$ at 550 °C (Table 1 and equation (5)), which possibly indicates a noticeable contribution of viscous relaxation to the dissipation observed at these temperatures.

Flexural forced-oscillation data, in the form of “normalised flexural compliance” and “specimen assembly phase lag” obtained at representative temperatures, are displayed in Figure A.2. Although the flexural forced-oscillation data (particularly the specimen assembly phase lag data) are significantly more scattered than their torsional counterparts, it is clear that the normalised flexural compliance increases with increasing temperature between room temperature and 500 °C (Figure A.2a). The data are too scattered to provide

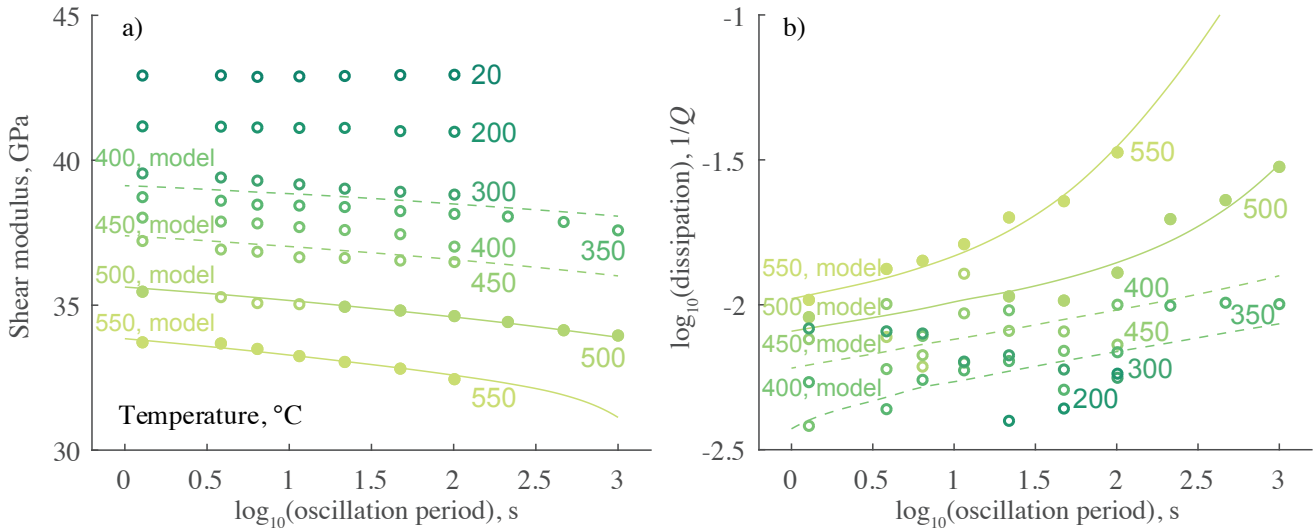


Figure 2. Shear modulus and dissipation data (symbols) and optimal Burgers model (curves) for antigorite. The scatter in the dissipation data provides an indication of experimental uncertainties (*n.b.* at room temperature, $\log_{10} Q_G^{-1} < -2.5$ at all oscillation periods). The Burgers model (see Table 1) was fitted to $N = 14$ (G, Q_G^{-1}) data pairs (full symbols) in the 500–550 °C temperature range and extrapolated to 450 and 400 °C (dashed curves).

any resolvable period-dependence for either the normalised flexural compliance and specimen assembly phase lag data. The flexural oscillation data are compared with the finite-difference approximation to the filament elongation model in Figure A.2. Importantly, the model relies on the assumption that the Young’s modulus, at each location along the temperature gradient, is prescribed by combining the complex shear modulus for specimen or alumina connecting rods and the copper jacket, previously determined in torsional forced-oscillation tests, with the corresponding *anharmonic temperature-dependent bulk modulus*. That the model predictions are in semi-quantitative accord with the observations indicates that such assumption is reasonable for the antigorite specimen. Recalling that the antigorite specimen tested here is isotropic, it follows that the Young’s modulus, E , and its associated attenuation, Q_E^{-1} for antigorite can be directly estimated as functions of temperature and oscillation period from shear modulus and associated attenuation data, respectively, as

$$E(T, T_0) = \frac{9K(T)G(T, T_0)}{3K(T) + G(T, T_0)}, \quad (7)$$

and, for complex elastic moduli with small imaginary components [Winkler and Nur, 1979],

$$Q_E^{-1} = \frac{E(T, T_0)}{3G(T, T_0)} Q_G^{-1}, \quad (8)$$

where K denotes bulk modulus. Note that the temperature-dependence of antigorite’s bulk modulus can be directly calculated from that experimentally measured for shear modulus (see below) by taking a temperature-independent Poisson’s ratio (an assumption which seems reasonable for antigorite [Christensen, 1996; Ji et al., 2013]) and using conversions between elastic constants.

4. Discussion and Conclusions

Our laboratory dataset provides new quantitative estimates of the temperature dependence of shear modulus G at seismic frequencies (mHz–Hz) in the antigorite stability

field. The shear velocity V_S and impedance Z_S are directly calculable as $V_S = \sqrt{G/\rho}$ and $Z_S = \sqrt{\rho G}$, respectively, where ρ is the rock density.

At room temperature, the shear modulus is independent of frequency (Figure 2a), a behaviour which is common in dry rocks at small strain amplitudes [Mavko, 1979; Jackson et al., 1992]. The shear modulus at room temperature ($G \approx 43$ GPa) is broadly comparable with those previously measured by ultrasonic techniques at the MHz frequency under similar confining pressures on the same material ($G = 37$ GPa, at 1.5 kbar [David et al., 2018]), on other isotropic antigorite-rich serpentinites ($G = 39$ GPa and $G = 34$ GPa, respectively, at 2 kbar [Simmons, 1964; Christensen, 1978]), or using aggregate averages from single-crystal elasticity data ($G = 38.5$ GPa, at room pressure [Bezacier et al., 2010]).

Relatively few data on the *temperature-dependence* of shear modulus (and, more generally, of seismic velocities) in antigorite are available. Christensen [1979] reports measurements of the compressional wave velocity V_P (at 2 kbar) and obtains $\partial V_P / \partial T = -0.68 \times 10^{-3} \text{ km s}^{-1} \text{ K}^{-1}$ in the 25–300 °C temperature range, a value that has often been used to account for the effect of temperature on seismic velocity in antigorite in the geophysical literature (*e.g.*, Carlson and Miller [2003]; Mookherjee and Capitani [2011]). However, we note that the data of Christensen [1979] were obtained on a chrysotile-rich (98%) serpentinite sample. The temperature dependence of P- and S-wave velocities can also be inferred from the data of Kern et al. [1997]. Although Kern’s data were obtained on a highly anisotropic antigorite serpentinite, the temperature dependence of the shear velocity is overall independent of the direction of both wave propagation and wave polarisation and averages $-0.4 \text{ km s}^{-1} \text{ °C}^{-1}$ in the 20–620 °C temperature range (at 1 kbar). In comparison, a linear fit to the shear modulus *vs.* temperature data of Figure 2a gives $\partial G / \partial T \sim -0.017 \text{ GPa K}^{-1}$ (at 1 s oscillation period). This estimate is more robust than the value of $\partial G / \partial T$ for the Burgers model (Table 1), which is associated with a significant uncertainty as the model was only fitted to the 500–550 °C data. Differentiation of the relation $V_S = \sqrt{G/\rho}$ with respect to temperature allows the temperature dependence of the shear velocity to be calculated from

that of shear modulus as:

$$\partial V_s / \partial T = \frac{\partial G / \partial T}{2\sqrt{\rho G}} + \frac{\alpha_v V_s}{2}, \quad (9)$$

where α_v is the volumetric coefficient of thermal expansion ($\alpha_v \approx 2.8 \times 10^{-5} \text{ K}^{-1}$ for antigorite [Holland and Powell, 1998]). This calculation yields $\partial V_s / \partial T = -0.76 \times 10^{-3} \text{ km s}^{-1} \text{ K}^{-1}$. This “low-frequency” temperature derivative of the shear velocity is higher than that inferred from the MHz measurements of Kern *et al.* [1997] — a result which is expected in a dispersive material. Finally, note that, in the 20–620 °C temperature range, the laboratory measurements of Kern *et al.* [1997] also provide direct estimates of $\partial V_p / \partial T$ averaging $-0.6 \text{ km s}^{-1} \text{ °C}^{-1}$ (at 1 kbar). Such a temperature derivative is very close to that measured by Christensen [1979] on chrysotile serpentine, which may indicate that the temperature-dependence of seismic velocities may be comparable among serpentine polytypes.

It is plausible that the time dependence of attenuation above 500 °C might originate from anelastic processes acting at grain boundaries, *i.e.*, from intergranular relaxation. This interpretation is first supported by the overall fine-grained nature of the material, along with its pronounced grain size and shape heterogeneity. This complex grain boundary morphology, combined with the strong elastic anisotropy of antigorite crystals [Bezacier *et al.*, 2010], will inevitably contribute to the stress concentrations on grain boundaries that are involved in elastically accommodated and diffusionally assisted grain-boundary sliding [Jackson *et al.*, 2014], captured here in the Burgers model by the wide distribution of anelastic relaxation times. The operation of an intragranular mechanism is also unlikely due to the difficulty in activating dislocation slip systems in antigorite without very high differential stresses [Auzende *et al.*, 2015]. Furthermore, laboratory observations suggest that dislocation damping in silicates (*e.g.*, in olivine) is usually only operative at temperatures significantly above the antigorite stability field [Guéguen *et al.*, 1989; Farla *et al.*, 2012]. In addition, the value of activation energy (268 kJ mol^{-1}) obtained in this study is an order of magnitude higher than those of Hilairet *et al.* [2007] for moderate to large strain dislocation-based deformation in antigorite at high confining pressures $\geq 10 \text{ kbar}$ (9 to 60 kJ mol^{-1} depending on flow law and pressure range), although large uncertainties are attached to the values of activation energy in both studies. Nevertheless, we also suggest that some viscoelastic relaxation might be concentrated within the antigorite grains, involving dislocation slip within the (001) “corrugated” cleavage plane, or possibly along weak conjugate planes making a small angle to the basal (001) plane and formed by weak OH bonds located between tetrahedral and octahedral sheets [Amiguet *et al.*, 2014]. Considering the high difficulty of identifying the relaxation mechanisms responsible for the observed anelasticity at the microscopic level, a more definitive mechanistic interpretation would notably require further experimental studies looking for a grain-size dependence, and knowledge of activation energy for elementary mechanisms such as grain boundary diffusion or self-diffusion. Although no evidence of dehydration is observed in the antigorite specimen recovered after the experiment, the present experimental conditions (confining pressure of 2 kbar, maximum temperature of 550 °C) are at or beyond the thermodynamic stability field of antigorite [Ulmer and Trommsdorff, 1995]. Therefore, regardless of the specific mechanism responsible for anelastic relaxation, it is possible that the noticeable increase of attenuation above 500 °C

is caused by enhanced diffusion kinetics near the dehydration temperature in metastable antigorite.

The geophysical significance of the present study is highlighted by comparing the new shear modulus and attenuation data in antigorite (Figure 2) with existing data in the same temperature range in *olivine*, the most abundant mineral in the Earth’s upper mantle. The data of Jackson and Faul [2010] and Jackson *et al.* [2014] reveal that olivine is essentially elastic in its behaviour at temperatures lower than 800 °C, with $G > 60 \text{ GPa}$ and $\log_{10} Q_G^{-1} \ll -2.0$. The contrasting seismic properties between antigorite and olivine can be summarised as follows. (i) Antigorite’s shear modulus is approximately 50–60% of that of olivine at all temperatures. For instance, at 400 °C and 10 s oscillation period, the shear moduli for antigorite and olivine are 37.7 and 65 GPa (Jackson *et al.* [2014], Fig. 4), respectively. Taking densities of 3.32×10^3 and $2.65 \times 10^3 \text{ kg m}^{-3}$ yields S-wave velocities of 3.77 and 4.42 km s^{-1} , respectively. The resulting contrasts in shear velocity and impedance are substantial: about 17% and 47%. (ii) The shear modulus is clearly more temperature-dependent in antigorite than in olivine. At 1 s oscillation period, the shear modulus of antigorite decreases by about 21% between room temperature and 550 °C, whereas the corresponding decrease in the shear modulus of olivine is only about 13%. (iii) Attenuation is higher in antigorite than in olivine, *e.g.*, at 550 °C and 100 s oscillation period, $\log_{10} Q_G^{-1} \approx -1.5$ for antigorite, whereas for olivine $\log_{10} Q_G^{-1} \ll -2.0$ below 800 °C. A similar observation holds if dissipation data for antigorite are compared with measured values of $\log_{10} Q_G^{-1} \approx -2.0$ on a ~80% olivine-rich dunite under comparable conditions (Jackson *et al.* [1992], Fig. 5d).

Our study reports new laboratory measurements of seismic velocity and attenuation in antigorite serpentine at various temperatures in laboratory conditions as close as possible to the propagation of seismic waves in the lithosphere. It is noteworthy that the Q^{-1} here measured in antigorite is comparable to those inferred seismologically in the mantle wedge-subducting slab region in subduction zones [see *e.g.* Pozgay *et al.*, 2009]. The contrast in shear velocity between antigorite and olivine is significant and consistent with the commonly accepted view that the presence of serpentine is associated with velocities that are lower than in peridotites. Attenuation is higher in antigorite than in olivine, but such contrast is much less than the shear velocity contrast.

Acknowledgments. The UK Natural Environment Research Council supported this work through grants NE/K009656/1 to NB and NE/M016471/1 to NB and TMM. This work has been enriched by discussions and help from Thomas Mitchell (UCL), and discussions with Greg Hirth (Brown University). Hayden Miller and Harri Kokkonen (ANU) provided technical support. The help of Christopher Cline (ANU) during experimental work and of Jackie Kendrick (University of Liverpool) during specimen preparation has been greatly appreciated. Ana Ferreira (UCL) provided useful comments on the manuscript. Experimental data are available from the UK National Geoscience Data Centre (<http://www.bgs.ac.uk/services/ngdc/>) or upon request to the corresponding author.

References

- Amiguet, E., B. V. de Moortèle, P. Cordier, N. Hilairet, and B. Reynard (2014), Deformation mechanisms and rheology of serpentines in experiments and in nature, *Journal of Geophysical Research*, 119, 4640–4655.
- Auzende, A.-L., J. Escartin, N. Walte, S. Guillot, G. Hirth, and D. Frost (2015), Deformation mechanisms of antigorite serpentine at subduction zone conditions determined from experimentally and naturally deformed rocks, *Earth and Planetary Science Letters*, 411, 229–240.

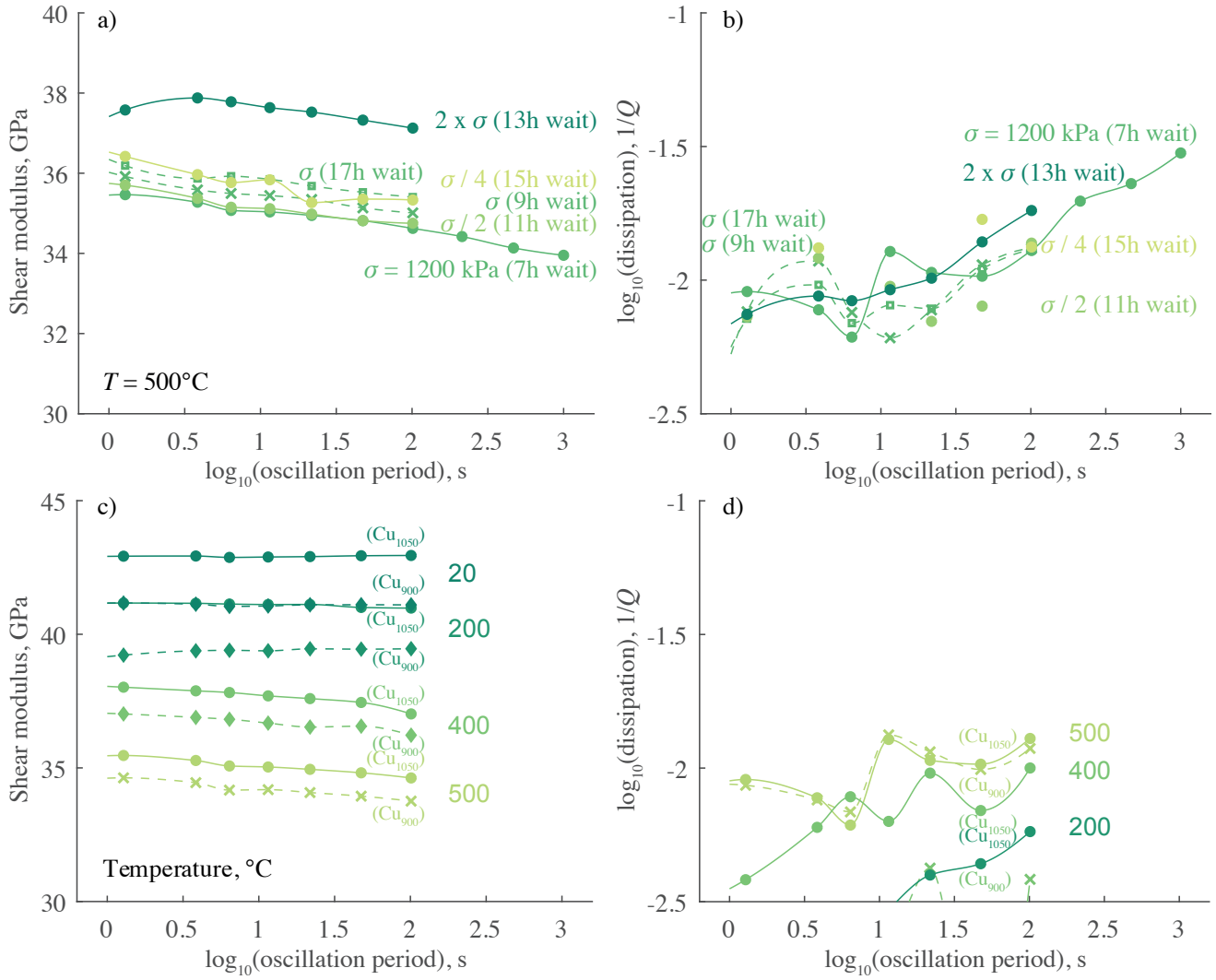


Figure A.1. a,b) Shear modulus and dissipation data for antigorite for various forced-oscillation tests at 500 °C, documenting temporal evolution and stress amplitude dependence of the mechanical behaviour with increasing exposure. The indicated stresses are maximum values pertaining to the cylindrical surface of the specimen. c,d) Sensitivity of shear modulus and dissipation data to corrections for the viscoelasticity of the copper jacket enclosing the antigorite specimen, at selected temperatures. The viscoelastic properties of copper after annealing at 900 °C (Cu_{900}) and 1050 °C (Cu_{1050}) were taken from *David and Jackson* [2018] (note that the viscoelastic properties of Cu_{900} at 500 °C were calculated by interpolating data between 600 and 400 °C).

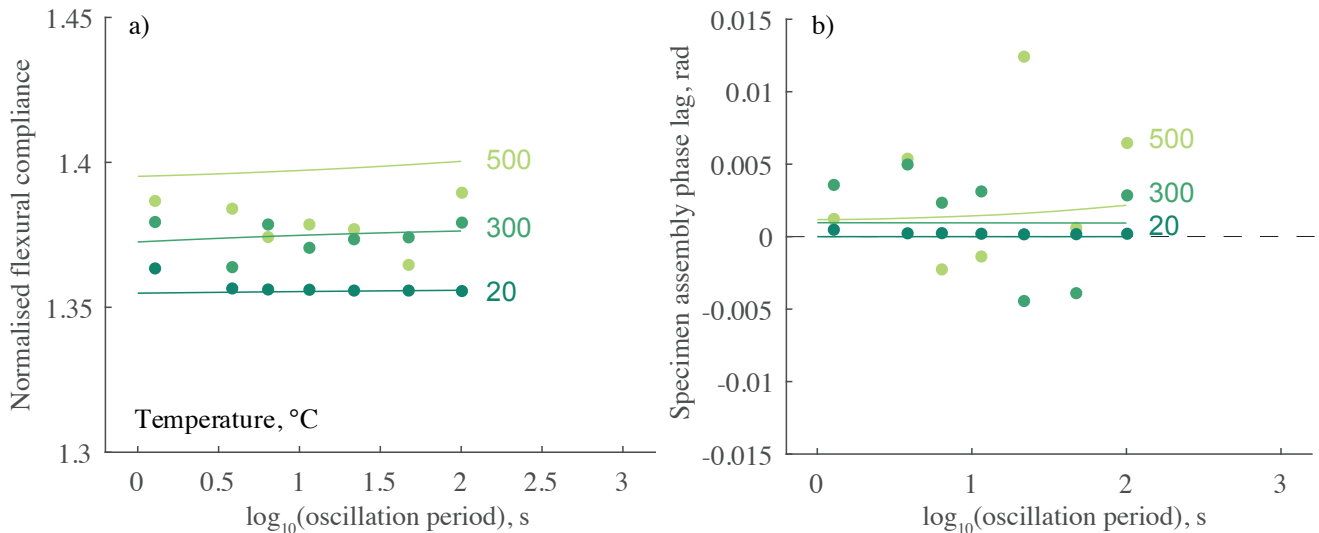


Figure A.2. Normalised flexural compliance and phase lag data (symbols) and flexure model (curves) for antigorite at representative temperatures.

- and *Planetary Science Letters*, 289, 198–208.
- Bezacier, L., B. Reynard, H. Cardon, G. Montagnac, and J. Bass (2013), High-pressure elasticity of serpentine and seismic properties of the hydrated mantle wedge, *Journal of Geophysical Research*, 118, 527–535.
- Birch, F. (1960), The velocity of compressional waves in rocks to 10 kilobars, part 1, *Journal of Geophysical Research*, 65, 1083–1102.
- Carlson, R., and D. Miller (2003), Mantle wedge water contents estimated from seismic velocities in partially serpentinized peridotites, *Geophysical Research Letters*, 30, 1250.
- Christensen, N. (1978), Ophiolites, seismic velocities and oceanic crustal structure, *Tectonophysics*, 47, 131–157.
- Christensen, N. (1979), Compressional wave velocities in rocks at high temperatures and pressures, critical thermal gradients, and crustal low-velocity zones, *Journal of Geophysical Research*, 84, 6849–6857.
- Christensen, N. (1996), Poisson's ratio and crustal seismology, *Journal of Geophysical Research*, 101, 3139–3156.
- Christensen, N. (2004), Serpentinities, peridotites, and seismology, *International Geology Review*, 46, 795–816.
- Cline, C., and I. Jackson (2016), Relaxation of the bulk modulus in partially molten dunite?, *Geophysical Research Letters*, 43, 11,644–11,651.
- Cline, C., U. Faul, E. David, A. Berry, and I. Jackson (2018), Redox-influenced seismic properties of upper-mantle olivine, *Nature*, 555, 7696.
- Cooper, R. (2002), Seismic wave attenuation: energy dissipation in viscoelastic crystalline solids, *Reviews in Mineralogy and Geochemistry*, 51, 253–290.
- David, E., and I. Jackson (2018), High-temperature internal friction and dynamic moduli in copper, *Materials Science and Engineering A*, 730, 425–437.
- David, E., N. Brantut, L. Hansen, and T. Mitchell (2018), Absence of stress-induced anisotropy during brittle deformation in antigorite serpentinite, submitted to *Journal of Geophysical Research*, e-Print archive on [arXiv.org](https://arxiv.org/abs/1806.08995), p. arXiv:1806.08995.
- Eberhard-Phillips, D., M. Chadwick, and S. Bannister (2008), Three-dimensional attenuation structure of central and southern South Island, New Zealand, from local earthquakes, *Journal of Geophysical Research*, 113, B05,308.
- Farla, R., I. Jackson, J. FitzGerald, U. Faul, and M. Zimmerman (2012), Dislocation damping and anisotropic seismic wave attenuation in Earth's upper mantle, *Science*, 336, 332–335.
- Guéguen, Y., M. Darot, P. Mazot, and Y. Woïgard (1989), q^{-1} of forsterite single crystals, *Physics of the Earth and Planetary Interiors*, 55, 254–258.
- Hilaret, N., B. Reynard, Y. Wang, I. Daniel, and S. Merkel (2007), High-pressure creep of serpentine, interseismic deformation, and initiation of subduction, *Science*, 318, 1910–1913.
- Holland, T., and R. Powell (1998), An internally consistent thermodynamic data set for phases of petrological interest, *Journal of Metamorphic Geology*, 16, 309–343.
- Hyndman, R., and S. Peacock (2003), Serpentinization of the forearc mantle, *Earth and Planetary Science Letters*, 212, 417–432.
- Jackson, I. (2015), *Properties of Rocks and Minerals: Physical Origins of Anelasticity and Attenuation in Rock*, vol. 2, 539–571 pp., Treatise on Geophysics, Elsevier.
- Jackson, I., and U. Faul (2010), Grainsize-sensitive viscoelastic relaxation in olivine: towards a robust laboratory-based model for seismological applications, *Physics of the Earth and Planetary Interiors*, 183, 151–163.
- Jackson, I., and M. Paterson (1993), A high-pressure, high-temperature apparatus for studies of seismic wave dispersion and attenuation, *Pure and Applied Geophysics*, 141, 445–466.
- Jackson, I., M. Paterson, and J. FitzGerald (1992), Seismic wave dispersion and attenuation in Åheim dunite: an experimental study, *Geophysical Journal International*, 108, 517–534.
- Jackson, I., A. Barnhoorn, Y. Aizawa, and C. Saint (2009), Improved procedures for the laboratory study of high-temperature viscoelastic relaxation, *Physics of the Earth and Planetary Interiors*, 172, 104–115.
- Jackson, I., H. Schijns, D. Schmitt, J. Mu, and A. Delmenico (2011), A versatile facility for laboratory studies of viscoelastic and poroelastic behaviour of rocks, *Review for Scientific Instruments*, 82, 064,501.
- Jackson, I., U. Faul, and R. Skelton (2014), Elastically accommodated grain-boundary sliding: New insights from experiment and modeling, *Physics of the Earth and Planetary Interiors*, 228, 203–210.
- Ji, S., A. Li, Q. Wang, C. Long, H. Wong, D. Marcotte, and M. Salisbury (2013), Seismic velocities, anisotropy, and shear wave-splitting of antigorite serpentinites and tectonic implications for subduction zones, *Journal of Geophysical Research*, 118, 1015–1037.
- Kern, H., B. Liu, and T. Popp (1997), Relationship between anisotropy of p and s wave velocities and anisotropy of attenuation in serpentinite and amphibolite, *Journal of Geophysical Research*, 102, 3051–3065.
- Mavko, G. (1979), Frictional attenuation: an inherent amplitude dependence, *Journal of Geophysical Research*, 84, 4769–4775.
- Minster, J., and D. Anderson (1981), A model of dislocation-controlled rheology for the mantle, *Philosophical Transactions of the Royal Society of London*, 299, 319–356.
- Mookherjee, M., and G. Capitani (2011), Trench parallel anisotropy and large delay times: elasticity and anisotropy of antigorite at high pressures, *Geophysical Research Letters*, 38, L09,315.
- Pozgay, S., D. Wiens, J. Conder, H. Shiobara, and H. Sugioka (2009), Seismic attenuation tomography of the Mariana subduction system: Implications for thermal structure, volatile distribution, and slow spreading dynamics, *Geochemistry, Geophysics, Geosystems*, 55, GC002,313.
- Reynard, B. (2013), Serpentine in active subduction zones, *Lithos*, 178, 171–185.
- Simmons, G. (1964), Velocity of shear waves in rocks to 10 kilobars, 1, *Journal of Geophysical Research*, 69, 1123–1130.
- Svitek, T., V. Vavryuk, T. Lokajicek, M. Petruzalek, and H. Kern (2017), Effect of pressure on 3D distribution of P-wave velocity and attenuation in antigorite serpentinite, *Geophysics*, 82, WA33–WA43.
- Ulmer, P., and V. Trommsdorff (1995), Serpentine stability to mantle depths and subduction-related magmatism, *Science*, 268, 858–861.
- Wang, Z., D. Zhao, X. Liu, C. Chen, and X. Li (2017), P and S wave attenuation tomography of the Japan subduction zone, *Geochemistry, Geophysics, Geosystems*, 18, 1688–1710.
- Watanabe, T., H. Kasami, and S. Ohshima (2007), Compressional and shear wave velocities of serpentinized peridotites up to 200 MPa, *Earth Planets and Space*, 59, 233–244.
- Winkler, K., and A. Nur (1979), Pore fluids and seismic attenuation in rocks, *Geophysical Research Letters*, 6, 1–4.

E.C. David, Department of Earth Sciences, University College London, Gower Street, London WC1E 6BT, UK. (e.david@ucl.ac.uk)